Research article

Sangeeta Rout, Samantha R. Koutsares, Devon Courtwright, Ezekiel Mills, Ayanna Shorter, Srujana Prayakarao, Carl E. Bonner and Mikhail A. Noginov*

Effect of nanoscale dielectric environments on concentration quenching

https://doi.org/10.1515/nanoph-2021-0132
Received March 27, 2021; accepted July 5, 2021;
published online August 2, 2021

Abstract: We have studied the dependence of concentration quenching of luminescence (donor–acceptor energy transfer) on the thickness d of dye-doped polymeric films (HITC:PMMA) and found its strong inhibition at small values of d. This phenomenon is tentatively explained by a limited number of acceptors, which donors' excitation can reach in thin samples, if the film's thickness is comparable to the diffusion length of the energy transfer. The latter mechanism, along with effective reduction of the dye concentration, is responsible for an inhibition of the concentration quenching of dye molecules impregnating porous alumina membranes. The elongation of emission kinetics in thick (≥3 μm) HITC:PMMA films is cautiously attributed to the samples' crystallinity.

Keywords: concentration quenching; diffusion length; emission kinetics; Förster radius.

1 Introduction

Energy transfer between donors and acceptors [1] (which can be atoms, molecules, quantum dots, etc.) is an important physical phenomenon, whose applications range from biophysics [2] and phosphors [3] to laser technology [4, 5] and photovoltaics [6]. The common utilizations of the energy transfer in technology include sensitization of emission [4, 5, 7] and photon cutting [8, 9] (also known as cross relaxation [4, 5]). Depending on emission and absorption spectra of donors and acceptors, their oscillator strengths, the rates of dephasing and relaxation, molecular concentrations, etc., energy transfer can be coherent or incoherent and reversible or irreversible [1]. The most common and thoroughly studied is the energy transfer occurring in the weak coupling Forster regime, which is incoherent and irreversible, and whose rate is determined by the overlap of the emission spectrum of donors and the absorption spectrum of acceptors [1, 10]. When the rate of the energy transfer, commonly resulting in quenching of donors' luminescence, increases with an increase of the molecular concentration, this phenomenon (primarily studied in this work) is referred to as the concentration quenching.

Quantum emitters [11, 12], including dye molecules [13, 14], are widely used in a variety of nanophotonics [15, 16] fundamental studies [17, 18] and applications [19, 20]. At high dye concentrations, which are of importance at stimulated emission [21, 22] and strong coupling [23–26], the concentration quenching of luminescence and its inhibition in vicinity to metallic surfaces and lamellar metal/dielectric metamaterials have been studied [27–29]. While the particular focus of these and other studies [30] was on effects of non-local metallic environments, the effects of the nanoscopic samples' geometry on luminescence kinetics in purely dielectric systems received much less attention. In this study, we have demonstrated and explained the dependence of luminescence concentration quenching and its inhibition on the (i) thickness of dye-doped polymeric films deposited on glass substrates and (ii) concentration of dye molecules impregnating porous anodic alumina membranes. Both effects are discussed in terms of the reduced number of acceptors available to donors in thin films and fibers. Furthermore, the (iii) experimentally observed elongation of emission kinetics in thick (≥3 μm) HITC:PMMA films is cautiously attributed to the samples' crystallinity.

***Corresponding author: Mikhail A. Noginov**, Center for Materials Research, Norfolk State University, Norfolk, VA 23504, USA, E-mail: mnoginov@nsu.edu
Sangeeta Rout, Samantha R. Koutsares, Devon Courtwright, Ayanna Shorter, Srujana Prayakarao and Carl E. Bonner, Center for Materials Research, Norfolk State University, Norfolk, VA 23504, USA.
https://orcid.org/0000-0002-6538-9489 (S. Rout)
Ezekiel Mills, Virginia State University, Petersburg, VA 23806, USA

2 Experimental samples

The experimental samples in our studies were (1) PMMA polymeric films doped with HITC dye, deposited on glass, and (2) anodic alumina membranes impregnated with dye-doped polymer (HITC:PMMA), Figure 1. The latter 50 μm thick membranes (acquired from Redox Inc.) had 30 ± 5 nm wide open pores (filling factor f = 15%), propagating wall-to-wall, perpendicular to the membrane's faces. The dye concentration ranged between $\nu = 2g/l$ and $\nu = 40g/l$ (in solid state) and the film thickness (on glass) varied between 11 nm and 3.6 μm.

The samples were prepared by dissolving 2-[7-(1,3-dihydro-1,3,3-trimethyl-2*H*-indol-2-ylidene)-1,3,5-heptatrienyl]-1,3,3-trimethyl-3*H*-indoliumiodide (HITC) dye and poly (methyl methacrylate) (PMMA) polymer in dichloromethane (DCM). The solution was then sonicated for t = 90 min at room temperature. Finally, the dye doped polymer solutions were spin coated onto micro glass slides (obtained from VWR International) or anodic alumina membranes, discussed above, Figure 1, using a spin-coater from Specialty Coating Systems (Model P6700). The thickness measurements of the polymeric films (on glass) were done using a stylus profilometer (Bruker Dektak XT).

3 Results and discussions

3.1 Spectroscopic and kinetics studies

The spectroscopic properties of HITC:PMMA films were studied in recent Ref. [27]. The emission and excitation spectra were collected using the spectrofluorimeter Fluorolog 3 (from Horiba) and the absorption spectra were taken using the spectrophotometer Lambda 900 (form PerkinElmer). Similar measurements were carried out in the present study. The absorption and excitation bands have the maxima at 762 nm, while the emission band has its peak position at 772 nm, Figure 2. Knowing the spectrum of absorption coefficients and the dye concentration, we have determined the spectrum of absorption cross sections $\mu(\omega)$.

In the emission kinetics measurements, the samples were excited with ~150 fs pulses of a mode locked Ti:Sapphire laser (Mira 900 from Coherent). The laser spot was ~ 2.5 mm in diameter, the average power was ~ 60 mW, and the repetition rate was 76 MHz. The emission kinetics were recorded using a visible and near-IR streak camera (Model C5680 from Hamamatsu). The time resolution, determined by the jitter of the laser and the wide-open entrance slit of the streak camera, was ~100 ps. The emission decay rates were determined by fitting the experimental kinetics with exponential functions, as explained below.

3.2 Donors and acceptors

In our experiments, not aggregated HITC dye molecules serve as donors. Quenching centers (acceptors) are, generally, of different nature and their concentration c_A can be either dependent on or independent of the molecular concentration ν, $c_A \propto \nu^x$, where x = 0, 1, 2, … Quadratic

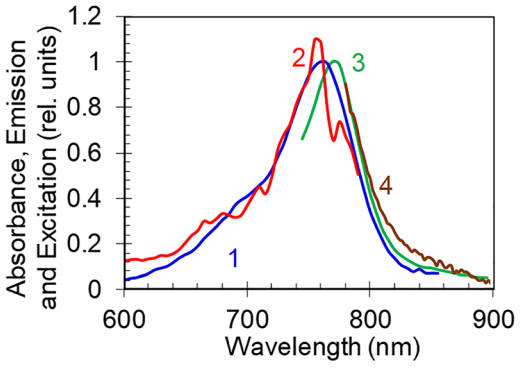

Figure 2: Absorption (trace 1), excitation (trace 2) and cw emission (trace 3) spectra of HITC:PMMA film on the glass substrate at a dye concentration of 8.5 g/l. Emission spectrum taken at short-pulse pumping (trace 4). Adopted from Ref. [27].

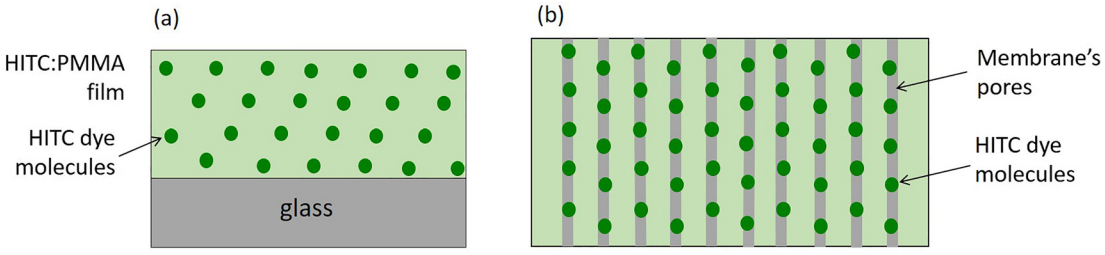

Figure 1: Schematics of experimental samples.
(a) HITC:PMMA film deposited on glass and (b) anodic alumina membrane impregnated with dye-doped polymer (HITC:PMMA).

dependence of the energy transfer rate on the HITC dye concentration, reported in Ref. [27], is consistent with $c_A \propto v^2$ and direct energy transfer between donors and acceptors [1], Figure 3a. On the other hand, at high concentration of donors c_D and efficient energy transfer between them, the migration of electronic excitation over donors can accelerate the energy transfer to acceptors and shorten donors' emission kinetics. In this case of migration-assisted energy transfer, Figure 3b, the quadratic dependence of the transfer rate on the dye concentration is predicted at $c_A \propto v$ [1]. We infer that the latter regime of donor–acceptor energy transfer takes place in our experiments, as described below.

3.3 Determination of the Förster radius

Knowing the experimental spectra of emission $F(\omega)$ and absorption cross section $\mu(\omega)$, we determined the Förster radius for energy migration over HITC molecules (the distance between two molecules at which the transfer rate is equal to the emission decay rate [1]) to be equal to

$$R_F^6 = \frac{9\chi^2 c^4 \eta}{8\pi} \int \frac{F(\omega)\mu(\omega)}{n^4\omega^4} d\omega = 5.3\,\text{nm}. \quad (1)$$

Here χ^2 is the factor describing relative orientation of dipoles ($\chi^2 = 2/3$ for random orientations) $\int F(\omega)d\omega = 1$, ω is the angular frequency, $n = 1.5$ [31] is the index of refraction, $\eta = 0.07$ [32] is the spontaneous emission quantum yield, and c is the speed of light. None of the features in the absorption spectra of HITC could be unambiguously attributed to acceptors. Therefore, the Forster radius for the donor–acceptor energy transfer could not be determined.

3.4 Emission kinetics of thin HITC:PMMA films on glass

In the emission kinetics analysis, we first treated all kinetics as single exponential and determined their effective decay rates γ by equating the area under the normalized experimental emission kinetics $\int_0^{t_{max}} \frac{I(t)}{I(0)} dt$ and the exponential function $\int_0^{t_{max}} \exp(-\gamma t)dt$, Figure 4a. As the root mean square error rms = $\sqrt{\frac{\sum_N (I(t)/I(0) - \exp(-\gamma t))^2}{N}}$ (determined by the experimental noise and deviation of the emission kinetics from exponential functions) propagated to the error of γ, it resulted in the error bars ranging from ≈1% to ≈5% – equal to or smaller than the sizes of the characters in Figure 5. The largest contribution to the experimental error of γ, ≈±10%, came from the sample-to-sample variation in the film fabrication and the error in the dye concentration v. (In the equation above, N is the number of the data points).

The emission kinetics of low concentrated HITC dye ($v = 2g/l$) deposited on glass substrates were nearly single exponential (Figure 4b) and their relatively small decay rates were practically independent of the film thickness (Figure 5, squares). A similar result was observed at $v = 3.6g/l$ in Ref. [27] (Figure 5, diamonds). According to Ref. [27], at this low dye concentration, the emission decay is predominantly determined by the combination of radiative and nonradiative intracentral relaxation processes, and the effect of the concentration quenching is small.

At the same time, at large dye concentrations, the emission kinetics had significantly higher decay rates (larger at $v = 40g/l$ than at $v = 30g/l$) and deviated from exponential functions (Figures 4a and b). This behavior is consistent with the concentration quenching of HITC molecules reported in Ref. [27]. (Note that the emission decay rates in our experiment did not increase with increase of the pumping intensity, ruling out energy transfer upconversion [33] as the key mechanism of the concentration quenching.)

At the dye concentration equal to v = 40 g/l, the emission kinetics were measured at various thicknesses of HITC:PMMA films, ranging from 11 nm to 3.6 μm. In the data set represented by solid black circles in Figure 5, the film thickness was controlled by viscosity of the solution at unchanged spinning parameters. The corresponding emission decay rates were maximal at the film thicknesses $d \sim 1$ μm and they decreased significantly at smaller values of d. The characteristic length scale of the decay rate reduction, d_0 = 33 nm, was determined by fitting the data

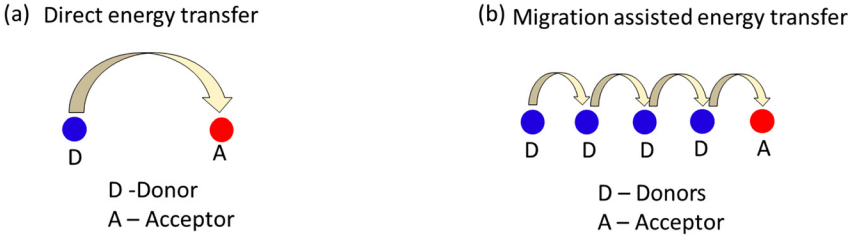

Figure 3: Schematics of direct (a) and migration-assisted (b) energy transfer.

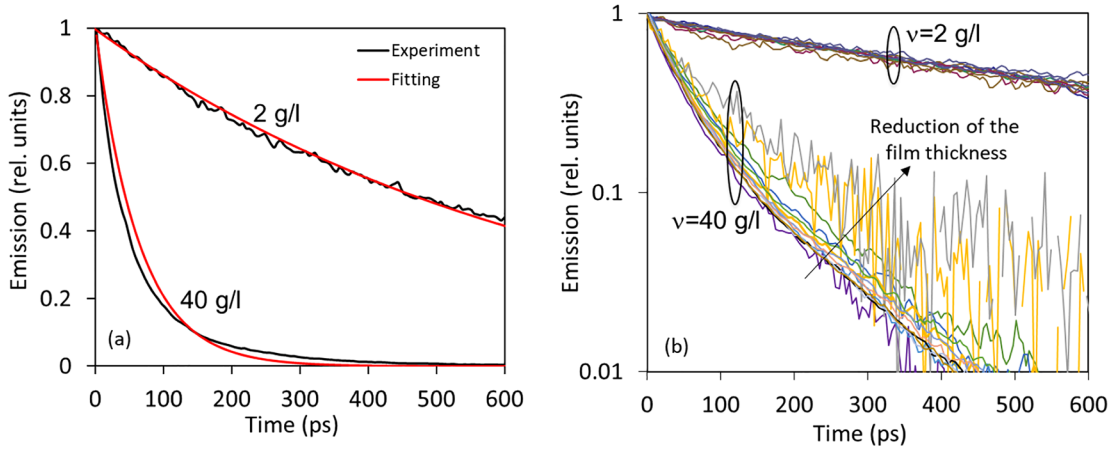

Figure 4: (a) Experimental emission kinetics at low $v = 2$ g/l and high $v = 40$ g/l dye concentrations and their fits with exponential functions. (b) Emission kinetics of HITC:PMMA films deposited on glass at the film thicknesses ranging from $d = 15$ nm to $d = 364$ nm at low dye concentration $v = 2g/l$ (adopted from Ref. [28]) and from $d = 11$ nm to $d = 957$ nm at high dye concentration $v = 40g/l$.

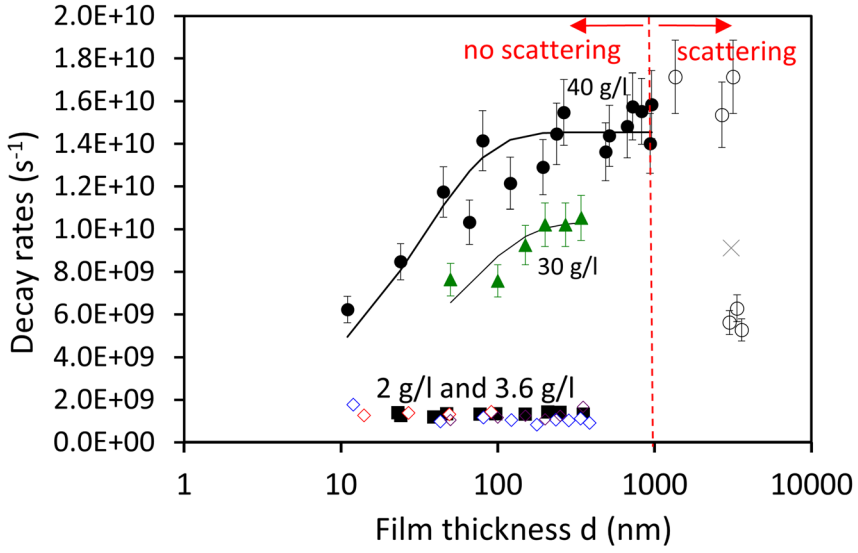

Figure 5: Dependence of the emission decay rates in HITC:PMMA films as the function of the film thickness d; $v = 40g/l$: Filled black circles (varied viscosity), open black circles (varied spinning rate), cross (drop casting), sold line – fitting with formula $C + B(1 - \exp(-d/d_0))$; $v = 30g/l$: Green triangles, sold line – fitting with formula $C + B(1 - \exp(-d/d_0))$; $v = 3.6g/l$: Open red, blue, and purple diamonds; $v = 2g/l$: Filled black squares. Vertical dashed line shows an onset of scattering. The error bars are shown.

points with the function $C + B(1 - \exp(-d/d_0))$, solid line in Figure 5. A qualitatively similar behavior (and the fitting) have been demonstrated in the series of HITC:PMMA films with dye concentrations equal to $v = 30g/l$, green triangles in Figure 5.

3.5 Diffusion length of the excitation migration

We infer that shortening of the emission kinetics in thin films (at high dye concentrations) is due to a relatively small number of acceptors to which donors can transfer their excitation, leading to inhibition of the Förster energy transfer and inhibition of the concentration quenching. Naively, one would think that this effect can be significant only at film thickness $d \le R_F$. However, as we show below, the characteristic length of the excitation migration can be larger than this. We assume that the energy migration over donors (delivering excitation energy to acceptors) is diffusion, with the diffusion coefficient (in 1D approximation) given by [34]

$$D = \frac{1}{2}\frac{R^2}{\Delta t} = \frac{1}{2\tau_0}\frac{R_F^6}{R^4} \tag{2}$$

where Δt is the time of the excitation "hop" between two molecules, related to the energy transfer rate W as $\Delta t = 1/W = \tau_0 (R/R_F)^6$, τ_0 is the emission decay time, R_F is the Forster radius, and $R = v_0^{-1/3}$ is the average distance between molecules. (Here v_o the concentration in cm^{-3}. For HITC:PMMA, $v = 1$ g/l is equivalent to $v_0 = 1.83 \times 10^{18}$ cm^{-3}). Correspondingly, the characteristic diffusion length [34]

(the standard deviation of the diffusion spread of excitation) is equal to

$$\sigma = \sqrt{2Dt} = \frac{R_F^3}{R^2}\sqrt{\frac{t}{\tau_0}} \tag{3}$$

Thus, at $t = \tau_0$ (time interval equal to the excitation lifetime),

$$\sigma(\tau_0) = R_F^3/R^2 = R_F^3 v_0^{2/3} \tag{4}$$

Therefore, $\sigma(\tau_0)$ grows with increase of both the Forster radius and the donors' concentration.

At $v = 40g/l$: $v_0 = 7.32 \times 10^{19}$ cm^{-3}, $R = 2.7$ nm, and $\sigma(\tau_0) = nm$. This means that during the luminescence lifetime, excitation migrates over 20 nm, making many "hops" from donor to donor before terminating at an acceptor, which can be as far as 20 nm away from the originally excited donor. This scenario of migration-assisted energy transfer [1] is consistent with the quadratic dependence of the concentration quenching on the dye concentration reported in Ref. [27]. Correspondingly, the energy transfer occurring within 20 nm from the film's surface is sensitive to the existence of the boundary of the dye-doped medium and absence of acceptors outside of the dye-doped film. As each film has two surfaces, the net volume affected by the vicinity to the interfaces is 40 nm thick, nearly an order of magnitude larger than the Forster radius $R_F = 5.3$ nm and close to $d_0 = 33$ nm determined experimentally. (Note that at the emission quantum yield η exceeding 0.07, the Forster radius R_F and the characteristic diffusion length $\sigma(\tau_0)$ will be even larger.)

3.6 Inhibition of concentration quenching in anodic alumina membranes

In the next particular experiment, we impregnated anodic alumina membranes with HITC:PMMA at different dye concentrations v and studied the emission kinetics and the decay rates as the function of v. The ~80 nm dye-doped polymeric films with the same dye concentrations, deposited on glass, served as control samples.

In accord with Ref. [27], the HITC:PMMA films on glass demonstrate growth of the emission decay rates with increase of v (concentration quenching) that could be fitted with the formula $(A + W) + \gamma v^2$, Figure 6. Here $(A + W)$ is the rate of radiative and nonradiative intracentral relaxation and γ is the rate of the concentration quenching.

In membrane samples impregnated with HITC:PMMA at *low* dye concentrations, the decay rates were almost similar to those in the control samples (at the same dye concentrations). However, at *high* dye concentrations, the decay rates in membranes were significantly smaller than those in the HITC:PMMA films on glass, Figure 6.

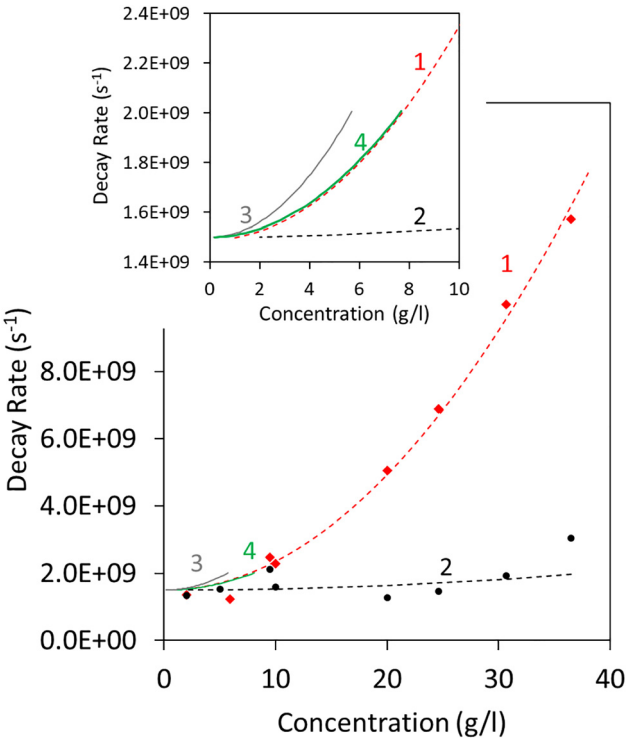

Figure 6: Concentration dependence of the emission decay rate in HITC:PMMA on glass (trace 1: Red diamonds and red dashed line) and in anodic alumina membranes (trace 2: Black circles and black dashed line). The dashed lines are the best fits of the experimental points with formula $(A + W) + \gamma v^2$. Traces 3 and 4: Same as trace 2 but, plotted against the scaled concentrations fv rather than the original concentration v. Trace 3: $f = 0.15$, poor match with trace 1. Trace 4: $f = 0.20$, good agreement with trace 1. Inset: Zoomed part of the main frame.

Based on the model of the excitation migration discussed above, we argue that ~30 nm in diameter HITC:PMMA polymer fibers formed in pores of alumina membranes were so thin that they inhibited the long-range diffusion energy transfer and the corresponding concentration quenching. One can further infer that the statistically uniform distribution of the nanometer-scale HITC:PMMA dispersed phase is equivalent to a reduced dye concentration fv, where f is the filling factor for a dye-doped polymer.

The reduction of the effective dye concentration fv causes the reduction of the concentration quenching and qualitatively explains the experimental result of Figure 6. In this figure, the decay rates in HITC:PMMA on glass (trace 1) and in alumina membrane (trace 2) are plotted against the dye concentration v. Traces 3 and 4 depict the decay rates of HITC:PMMA in alumina membrane plotted against

scaled concentrations $f_1\nu$ and $f_2\nu$, respectively. Here $f_1 = 0.15$ is equal to the pores' filling factor in the alumina membrane and $f_2 = 0.20$ is the effective concentration scaling factor providing for the best match of traces 1 and 4. The fact that trace 1 (dye on glass) can be fitted with trace 4 (dye in membrane plotted against scaled concentration) suggests that the porous environment, in the first approximation, is equivalent to reduction of the dye concentration. However, the mismatch between trace 3 (corresponding to the expected filling factor $f = 0.15$) and trace 1 (experimental decay rates on top of glass) indicates that the analogy is incomplete.

The same mechanism is also expected to contribute to inhibition of concentration quenching in thin films in vicinity of metallic nanostructures [27–29, 35]. However, the inhibition of the concentration quenching in metallic nanostructures is stronger than that on top of glass [28].

3.7 Inhibition of concentration quenching in thick HITC:PMMA films

Another intriguing phenomenon was observed in thick highly doped HITC:PMMA films ($d \geq 3.0$ μm, $\nu = 40\,g/l$), in which the decay rates dropped abruptly to approximately one third of their maximal value at ~1 μm (Figure 5, open circles). The thick samples, starting from $d \geq 0.96$ μm, were scattering (milky), as opposed to clear slightly colored thinner films. All thick samples with reduced decay rates were scattering. However, not all scattering samples (in the range 1 μm ≤ d ≤ 3 μm) had reduced decay rates, Figure 5. Furthermore, thick samples with reduced decay rates had anomalously strong absorption, nearly 10 times larger than that in samples of comparable thickness with uninhibited emission decay, Figure 7. The milkiness of the thick films

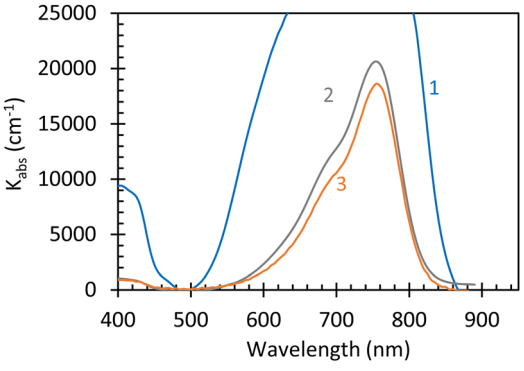

Figure 7: Absorption spectrum of the scattering 3.0 μm HITC:PMMA film (trace 1), not scattering 2.68 μm film (trace 2), and not scattering 0.24 μm film (trace 3). Dye concentration: $\nu = 40$ g/l.

can be due to known in the literature crystallinity of PMMA [36], which can depend on the processing conditions, such as varied spinning rates used for the fabrication of thick samples. At the same time, the effect of crystallinity on the anomalously strong absorption and the inhibition of the concentration quenching are still waiting for their explanations.

4 Summary

To summarize, (i) we have studied the dependence of concentration quenching of luminescence (donor–acceptor energy transfer) on the thickness d of dye-doped polymeric films (HITC:PMMA) and found its strong inhibition at small values of d. (ii) This phenomenon is tentatively explained by the limited number of acceptors, which can be reached by donors' excitation in thin samples, if the film's thickness is comparable to the diffusion length of the energy transfer (determined by the Förster radius and the dye concentration). (iii) The same phenomenon is consistent with inhibition of the concentration quenching of dye embedded in anodic alumina membranes. (iv) The elongation of the emission kinetics in thick HITC:PMMA films is cautiously attributed to the samples' crystallinity.

According to Ref. [37], the photonic density of states (PDOS) and, correspondingly, the radiative decay rates of emitters implanted into a dielectric matrix are getting reduced in vicinity of a dielectric-air interface. The same mechanism should cause a reduction of spontaneous emission rates in thin HITC:PMMA films in our study. However, the comparison of the model [37] and our experiment suggests that the PDOS reasoning is insufficient to explain the strong reduction of the decay rates observed at high dye concentration $\nu = 40$ g/l (~2.5-fold, Figure 5). This and seeming absence of the PDOS effect in low doped HITC:PMMA thin films, $\nu = 2$ g/l and $\nu = 3.6$ g/l, is the subject of the further study to be published elsewhere.

Author contribution: All the authors have accepted responsibility for the entire content of this submitted manuscript and approved submission.
Research funding: The work was supported by National Science Foundation (NSF) grants 1830886 and 1856515, Air Force Office of Scientific Research (AFOSR) grant FA9550-18-1-0417, and Department of Defense (DoD) grant W911NF1810472.
Conflict of interest statement: The authors declare no conflicts of interest regarding this article.

References

[1] V. M. Agranovich and M. D. Galanin, "Electronic Excitation Energy Transfer in Condensed Matter," in *Modern Problems in Condensed Matter Sciences*, Amsterdam, North-Holland, Elsevier, 1982.

[2] D. L. Andrews and A. A. Demidov, *"Resonance Energy Transfer"*, Wiley, New York, 1999, ISBN 978-0-471-98732-1.

[3] K. Li, M. Shang, H. Lian, and J. Lin, "Recent development in phosphors with different emitting colors via energy transfer," *J. Mater. Chem. C*, vol. 4, pp. 5507–5530, 2016.

[4] R. C. Powell, *Physics of Solid-State Laser Materials*, vol. 1, New York, Springer Science & Business Media, 1998.

[5] A. A. Kaminskii, *"Laser Crystals: Their Physics and Properties"*, vol. 14, 2nd ed. Berlin, Heidelberg, Springer-Verlag, 1990.

[6] G. Chen, J. Seo, C. Yang, and P. N. Prasad, "Nanochemistry and nanomaterials for photovoltaics," *Chem. Soc. Rev.*, vol. 42, pp. 8304–8338, 2013.

[7] M. T. Nimmo, L. M. Caillard, W. De Benedetti, et al., "Visible to near-infrared sensitization of silicon substrates via energy transfer from proximal nanocrystals: further insights for hybrid photovoltaics," *ACS Nano*, vol. 7, pp. 3236–3245, 2013.

[8] B. M. van der Ende, L. Aarts, and A. Meijerink, "Near-Infrared quantum cutting for photovoltaics," *Adv. Mater.*, vol. 21, pp. 3073–3077, 2009.

[9] Y. Teng, J. Zhou, X. Liu, S. Ye, and J. Qiu, "Efficient broadband near-infrared quantum cutting for solar cells," *Opt Express*, vol. 18, pp. 9671–9676, 2010.

[10] T. Forster, "Intermolecular energy transfer and fluorescence," *Ann. Phys.*, vol. 2, pp. 55–75, 1948.

[11] I. Aharonovich, D. Englund, and M. Toth, "Solid-state single-photon emitter," *Nat. Photonics*, vol. 10, pp. 631–641, 2016.

[12] A. Delga, J. Feist, J. Bravo-Abad, and F. J. Garcia-Vidal, "Quantum emitters near a metal nanoparticle: strong coupling and quenching," *Phys. Rev. Lett.*, vol. 112, p. 253601, 2014.

[13] A. Mokhtari, A. Chebira, and J. Chesnoy, "Subpicosecond fluorescence dynamics of dye molecules," *J. Opt. Soc. Am. B*, vol. 7, pp. 1551–1557, 1990.

[14] E. Dulkeith, A. C. Morteani, T. Niedereichholz, et al., "Fluorescence quenching of dye molecules near gold nanoparticles: radiative and nonradiative effects," *Phys. Rev. Lett.*, vol. 89, p. 203002, 2002.

[15] R. J. Coles, D. M. Price, J. E. Dixon, et al., "Chirality of nanophotonic waveguide with embedded quantum emitter for unidirectional spin transfer," *Nat. Commun.*, vol. 7, pp. 1–7, 2016.

[16] P. N. Prasad, *"Nanophotonics"*, Hoboken, New Jersey, John Wiley & Sons Inc., 2004.

[17] V. A. G. Rivera, O. B. Silva, Y. Ledemi, Y. Messaddeq, and E. Marega Jr., *Collective Plasmon-Modes in Gain Media: Quantum Emitters and Plasmonic Nanostructures*, Cham; Heidelberg; New York; Dordrecht; London, Springer, 2014. Available at: https://doi.org/10.1007/978-3-319-09525-7.

[18] A. González-Tudela, P. A. Huidobro, L. Martín-Moreno, C. Tejedor, and F. J. García-Vidal, "Theory of strong coupling between quantum emitters and propagating surface plasmons," *Phys. Rev. Lett.*, vol. 110, p. 126801, 2013.

[19] Y. M. He, G. Clark, J. R. Schaibley, et al., "Single quantum emitters in monolayer semiconductors," *Nat. Nanotechnol.*, vol. 10, pp. 497–502, 2015.

[20] C. Polisseni, K. D. Major, S. Boissier, S. Grandi, A. S. Clark, and E. A. Hinds, "Stable, single-photon emitter in a thin organic crystal for application to quantum-photonic devices," *Opt Express*, vol. 24, pp. 5615–5627, 2016.

[21] M. A. Noginov, G. Zhu, A. M. Belgrave, et al., "Demonstration of a spaser-based nanolaser," *Nature*, vol. 460, pp. 1110–1112, 2009.

[22] M. A. Noginov, G. Zhu, M. Mayy, B. A. Ritzo, N. Noginova, and V. A. Podolskiy, "Stimulated emission of surface plasmon polaritons," *Phys. Rev. Lett.*, vol. 101, p. 226806, 2008.

[23] P. Törmä and W. L. Barnes, "Strong coupling between surface plasmon polaritons and emitters: a review," *Rep. Prog. Phys.*, vol. 78, p. 013901, 2014.

[24] J. Dintinger, S. Klein, F. Bustos, W. L. Barnes, and T. W. Ebbesen, "Strong coupling between surface plasmon-polaritons and organic molecules in subwavelength hole arrays," *Phys. Rev. B*, vol. 71, p. 035424, 2005.

[25] E. K. Tanyi, H. Thuman, N. Brown, S. Koutsares, V. A. Podolskiy, and M. A. Noginov, "Control of the Stokes shift with strong coupling," *Adv. Opt. Mater.*, vol. 5, p. 1600941, 2017.

[26] T. U. Tumkur, G. Zhu, and M. A. Noginov, "Strong coupling of surface plasmon polaritons and ensembles of dye molecules," *Opt Express*, vol. 24, pp. 3921–3928, 2016.

[27] S. Prayakarao, S. R. Koutsares, C. E. Bonner, and M. A. Noginov, "Effect of nonlocal metal–dielectric environments on concentration quenching of HITC dye," *J. Opt. Soc. Am. B*, vol. 36, pp. 3579–3587, 2019.

[28] S. Koutsares, L. S. Petrosyan, S. Prayakarao, et al., "Effect of metallic substrates and cavities on emission kinetics of dye-doped polymeric films," *J. Opt. Soc. Am. B*, vol. 38, pp. 88–94, 2021.

[29] V. N. Peters, S. Prayakarao, S. R. Koutsares, C. E. Bonner, and M. A. Noginov, "Control of physical and chemical processes with nonlocal metal–dielectric environments," *ACS Photonics*, vol. 6, pp. 3039–3056, 2019.

[30] F. Reil, U. Hohenester, J. R. Krenn, and A. Leitner, "Förster-type resonant energy transfer influenced by metal nanoparticles," *Nano Lett.*, vol. 8, pp. 4128–4133, 2008.

[31] M. Müller, R. Zentel, T. Maka, S. G. Romanov, and C. M. Sotomayor Torres, "Photonic crystal films with high refractive index contrast," *Adv. Mater.*, vol. 12, pp. 1499–1503, 2000.

[32] S. Prayakarao, D. Miller, D. Courtwright, C. E. Bonner, and M. A. Noginov, "Non-resonant enhancement of spontaneous emission of HITC dye in metal-insulator-metal waveguides," *J. Opt. Soc. Am. B*, vol. 36, pp. 2312–2316, 2019.

[33] F. Auzel, "Upconversion and anti-Stokes processes with f and d ions in solids," *Chem. Rev.*, vol. 104, pp. 139–174, 2004.

[34] H. Berg, "Chapter 1. Diffusion: Microscopic Theory." In *Random Walks in Biology*, Princeton, Princeton University Press, 2018, pp. 5–16.

[35] S. Rout, Z. Qi, L. S. Petrosyan, et al., "Effect of random nanostructured metallic environments on spontaneous emission of HITC dye," *Nanomaterials*, vol. 10, p. 2135, 2020.

[36] J. D. Stroupe and R. E. Hughes, "The structure of crystalline poly-(methyl methacrylate)," *J. Am. Chem. Soc.*, vol. 80, pp. 2341–2342, 1958.

[37] E. Snoeks, A. Lagendijk, and A. Polman, "Measuring and modifying the spontaneous emission rate of erbium near an interface," *Phys. Rev. Lett.*, vol. 74, pp. 2459–2462, 1995.